New Technology Reports

Special Articles on 1-Gbit/s Packet Signal Transmission Experiments toward Broadband Packet Radio Access

Configuration and Performances of Implemented Experimental Equipment

Noriyuki Maeda, Hiroyuki Kawai,
Junichiro Kawamoto and Kenichi Higuchi

We have conducted packet signal transmission experiments using MIMO multiplexing in a VSF-Spread OFDM radio access with a 100-MHz frequency bandwidth. The experimental results show that a 1-Gbit/s throughput is achieved at the average received E_b/N_0 (signal energy per bit-to-noise power spectrum density ratio) of about 12 dB by MIMO multiplexing with four transmitter and receiver antenna branches by applying a QRM-MLD signal detection method adopting adaptive selection of surviving symbol replica candidates, 16QAM data modulation, and soft-decision Turbo decoding with a coding rate of 8/9.

1. Introduction

We implemented experimental broadband packet radio access equipment that adopts a Multiple Input Multiple Output (MIMO) transmission method to achieve very high frequency efficiency of 10 bit/s/Hz [1][2]. Here, we describe the configuration of the experimental 1-Gbit/s packet signal transmission equipment, which adopts MIMO multiplexing with Variable Spreading Factor (VSF)-Spread Orthogonal Frequency Division Multiplexing (OFDM) radio access using a 100-MHz bandwidth in the downlink [3][4]. We also present the results of laboratory experiments using multipath fading simulators.

2. Experimental Setup

2.1 Overall Configuration

We are focusing on experimental packet signal transmission at up to 1 Gbit/s using MIMO multiplexing in 100-MHz-bandwidth downlink VSF-Spread OFDM radio access. First, we explain the configurations of the base station transmitter and the mobile station receiver. The implemented MIMO transmitter and receiver configurations are shown in **Figure 1** (a) and (b), respectively, and they adopt the major radio link parameters listed in **Table 1**. For downlink radio access, VSF-Spread OFDM access with a channel bandwidth of 101.5 MHz is used. In the base station transmitter, the serial binary information data bits are first serial-to-parallel converted to four streams corresponding to each transmitter antenna branch and then encoded using Turbo coding with a coding rate of R=1/2 to 8/9 and a constraint length of four bits. For the data modulation, Quadrature Phase Shift Keying (QPSK) modulation and 16 Quadrature Amplitude Modulation (16QAM) is used. The transmitter has four antenna branches. The transmitted symbol sequences for the transmitter antenna branches is interleaved in the OFDM frequency domain. The interleaved transmission

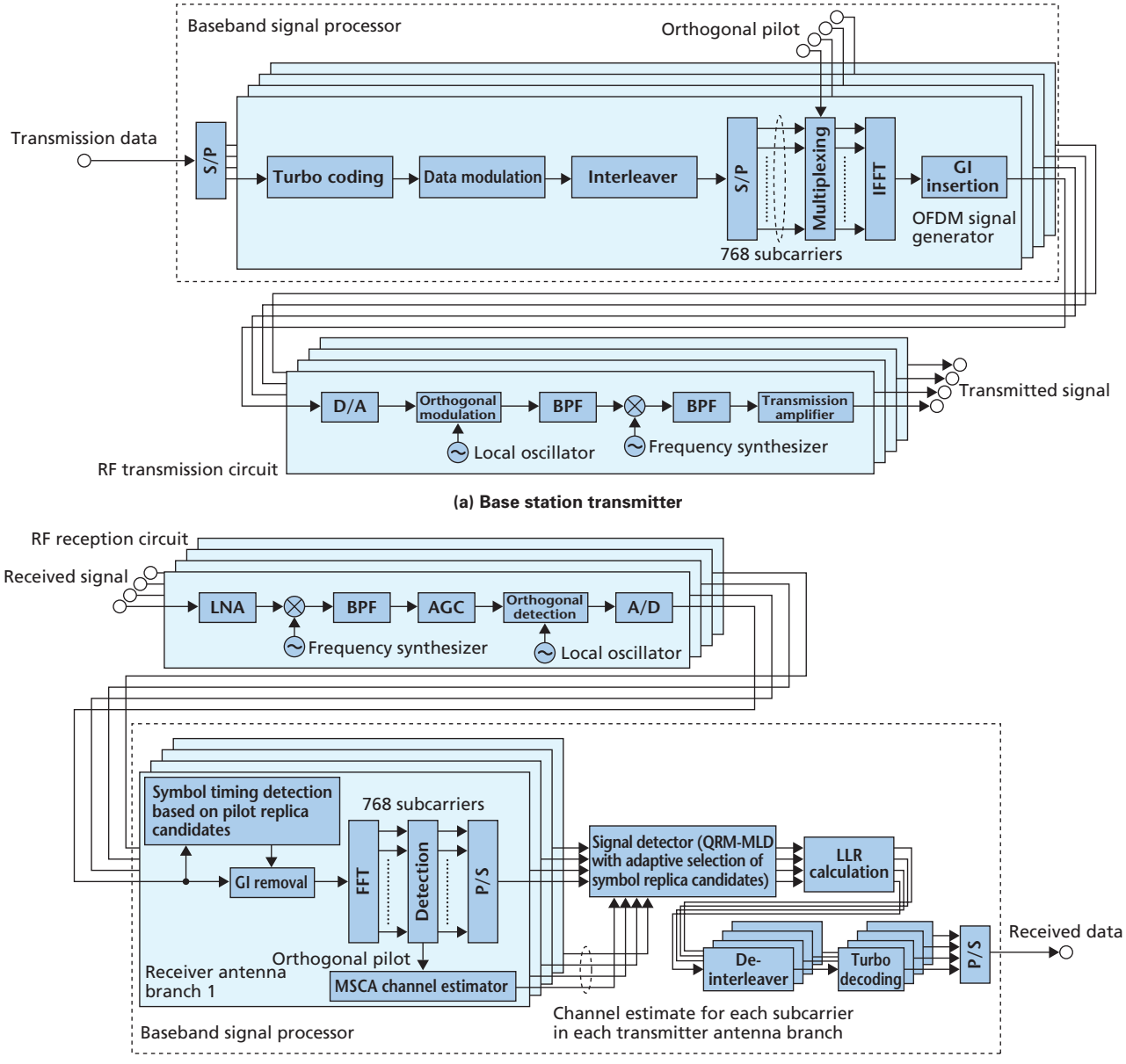

Figure 1 Configuration of implemented MIMO transmitter and receiver

Table 1 Basic specifications of the experimental system (downlink)

Radio access	VSF-Spread OFDM
Carrier frequency	4.635 GHz
Bandwidth	101.5 MHz
Transmitter and receiver antenna branches	4
Subcarriers	768 (131.836 kHz subcarrier interval)
OFDM symbol length	7.585 μs+GI 1.674 μs
Spreading factor	1
Data modulation	QPSK, 16QAM
Channel encoding and decoding	Turbo coding (R=1/2 to 8/9)/Max-Log-MAP decoding
Signal detection	QRM-MLD with ASESS

symbol sequence was converted to parallel signals for each subcarrier. Because symbol timing detection is performed in the receiver and since channel estimation is performed among the transmitter and receiver antenna branches, a four-symbol orthogonal pilot channel for each subcarrier and a two-symbol control channel are multiplexed within a 0.5-ms frame. The symbol stream for each transmitter antenna branch is converted to OFDM symbols (7.585 μs) for each transmitter antenna branch by 1024-point Inverse Fast Fourier Transform (IFFT) and a guard interval (1.674 μs) is appended. The subcarrier interval is 131.836 kHz. After conversion into baseband In phase (I) and Quadrature (Q) components by Digital-to-Analog (D/A) converters, quadrature modulation is performed. Finally, the Intermediate Frequency (IF) modulated signal is up-converted into the Radio Frequency (RF) signal where the center carrier frequency is 4.635 GHz and amplified by the power amplifier.

At the mobile station receiver, the frequency down-converted IF signal is first linearly amplified by an Automatic Gain Control (AGC) amplifier. The received spread signal is converted into baseband I and Q components by a quadrature detector. The I and Q signals are converted into digital format by the 12-bit Analog-to-Digital (A/D) converters. The OFDM symbol timing is estimated by taking the maximum cross-correlation peak between the received baseband digital signal and a reference signal such as a pilot symbol (this symbol timing is updated every 0.5 ms). After the guard interval is removed, 768 parallel data sequences are de-multiplexed by Fast Fourier Transform (FFT) processing from the multi-carrier signal with 768 subcarriers. The channel gain of each packet frame at each subcarrier is estimated using a Multi-Slot and sub-Carrier Averaging (MSCA) filter [5] using the orthogonal pilot channel. The channel estimation value is used to detect the signals in the signal detector and the Log Likelihood Ratio (LLR) is calculated for each bit in the LLR calculation unit for the soft-decision Turbo decoder. Finally, the LLR for each bit is input to the Max-Log-Maximum *A Posteriori* (MAP) Turbo decoder and the decoded data for each transmitter antenna branch is subjected to parallel-to-serial conversion to regenerate the transmitted signal stream.

2.2 Configuration of the Channel Estimator with MSCA Filter

The configuration of the channel estimator that adopts an MSCA filter is shown in **Figure 2**. In the MSCA channel estimation filter, a tentative channel estimation value between each transmitter antenna branch and receiver antenna branch is first obtained for each subcarrier by coherently averaging the four pilot symbols in one slot and one subcarrier. The final channel estimation values are then calculated for each subcarrier by coherent averaging of that tentative channel estimation weighted with real numbers α_{Freq} in the frequency domain and α_{Time} in the time domain between three adjacent subcarriers and three slots. The noise-averaging effect of the weighting coefficients of the MSCA channel estimation filter increases as the coefficients increase, but there is a trade-off, as tracking ability against fluctuation in fading decreases as the coefficients become larger.

2.3 Adaptive Selection of Surviving Symbol Replica Candidates Based on Maximum Reliability

This experimental system adopts Adaptive SElection of Surviving Symbol replica candidates (ASESS) [6] that is based on reliability information obtained by the complexity-reduced Maximum Likelihood Detection with QR decomposition and M-algorithm (QRM-MLD) method explained in this special article [7]. The ASESS comprises (1) the symbol ranking processing at each stage using quadrant detection and (2) ASESS processing that adopts the accumulated branch metric and symbol ranking information for the surviving symbol replica candidates up to that stage. The processing in each part is explained in the following sections.

1) Symbol Replica Ranking at Each Stage

Symbol ranking based on quadrant detection for each newly

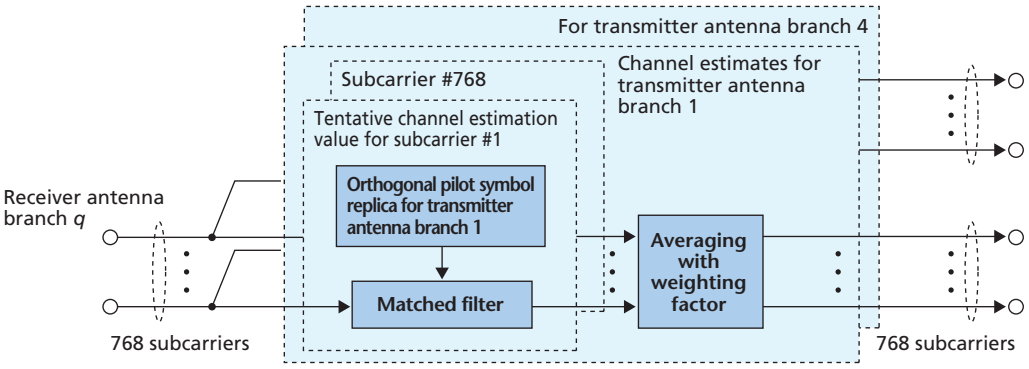

Figure 2 Configuration of the MSCA channel estimator

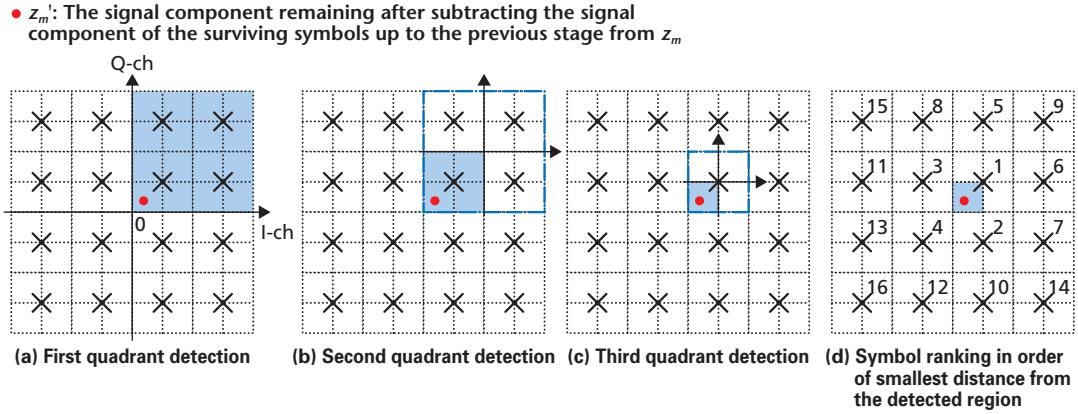

Figure 3 Symbol ranking based on quadrant detection

added symbol replica candidate at each stage is shown in **Figure 3**. An example of 16QAM data modulation case is shown. In the first stage of the QRM-MLD method, only the signal component (and noise component) of transmitted signal 1 is included in z_1. In addition, because the diagonal elements of matrix R derived by QR decomposition are always positive real numbers, phase rotation does not occur for z_1. Therefore, in step 1, the first quadrant detection is performed for z_1 and the quadrant for the position of z_1 is detected. The quadrant detection is only for confirming the signs of I and Q components of z_1, and can be done very simply. Next, the I and Q axes are moved to the center of the detected quadrant and the second quadrant detection is performed. By iterating this process N times, it is possible to determine in which of the $2^N \times 2^N$ regions of the partitioned signal constellation z_1 lies. In an actual system, the symbol ranking processing that adopts this quadrant detection can be implemented by storing the information on the signal constellation partitioning into $2^N \times 2^N$ regions in memory and identifying the region that contains z_1. Next, the symbol replica candidates are ranked in order of shortest distance from the center of the region in which z_1 lies. (Candidates that are equidistant from the region center are ranked in an order that has been decided in advance.) By applying this symbol ranking method, reliability information for each symbol can be obtained without calculating the squared Euclidian distance.

Furthermore, symbol ranking at stage m (m>1) is performed for the respective S_{m-1} surviving symbol replica candidates at stage (m–1), $c_{m-1,1},\ldots, c_{m-1,s_{m-1}}$. In the following, we explain symbol ranking for $c_{m-1,1}$. At stage m, z_m is a composite signal of the surviving symbols up to the previous stage and the symbols of that stage, so the signal newly added at that stage, z_m', can be generated by subtracting the $c_{m-1,1}$ signal component from z_m.

Then, by performing quadrant detection for z_m' in the same way as was done in the first stage, the 16 symbol replica candidates of transmitted signal m for $c_{m-1,1}$ are ranked in order of high reliability. By doing the same for the other surviving symbol replica candidates, $c_{m-1,2},\ldots, c_{m-1,s_{m-1}}$, symbol ranking of the 16 symbol replica candidates of the transmitted signal m is accomplished.

2) ASESS Based on Reliability Information from Iterative Processing

The operative principle of adaptive selection of surviving symbol replica based on reliability information is shown in

Figure 4, where the vertical axis is the accumulated branch metric, which represents the sum of the squared Euclidean distances of the surviving symbol replica candidates. The smaller the sum of the squared Euclidean distances (i.e., the smaller the accumulated branch metric), the higher the reliability of the symbol replica. Two types of reliability information can be applied at stage m (m>1). First, the accumulated branch metric information for the S_{m-1} surviving symbol replica candidates up to stage (m–1) are obtained. In Fig. 4, it is assumed that the accumulated branch metric is small and the reliability is high among the S_{m-1} surviving symbol replica candidates in the order of $c_{m-1,2}$,..., $c_{m-1,\,s_{m-1}}$. Next, the C symbol replicas added at stage m are ranked according to reliability by the previously described symbol ranking processing that adopts quadrant detection. In the ASESS proposed here, the candidates are selected in order of smaller accumulated branch metric (i.e., the smaller accumulated squared Euclidean distance) to serve as the surviving symbol replica candidates at stage m. In Fig. 4, because it is most likely that the sum of the squared Euclidean distance is smallest for the set of replicas of the surviving symbol replica, $c_{m-1,1}$ and the symbol replica added at stage m, $c_{m-1,1,1}$, the squared Euclidean distance is calculated from this set of symbol replica candidates. This accumulated squared Euclidean distance (the accumulated branch metric) is updated again as the accumulated branch metric of this set of symbol replica candidate. This value is also updated as a representative value of the accumulated branch metric for surviving symbol replica candidate $c_{m-1,1}$. Then, this is compared with the respective representative accumulated branch metrics of the other surviving symbol replica candidates $c_{m-1,2}$,..., $c_{m-1,\,s_{m-1}}$ from stage (m–1) (i.e., the accumulated branch metrics of the symbol replica candidates for which the accumulated branch metric of the S_{m-1} groups is minimum are compared). In the example of Fig. 4, because the combination of symbol candidate $c_{m-1,1,1}$ added to surviving symbol replica candidate $c_{m-1,1}$ has an even smaller accumulated branch metric than the representative symbol replica candidate of the other surviving symbol replica candidates $c_{m-1,2}$,..., $c_{m-1,\,s_{m-1}}$ (the smaller the accumulated branch metric, the higher the reliability), so next, the squared Euclidean distance is calculated for symbol candidate $c_{m-1,1,2}$, which is ranked next after $c_{m-1,1,1}$, and it is updated as the representative surviving symbol replica candidate for $c_{m-1,1}$. In the above way, for the S_{m-1} surviving symbol replica candidates, $c_{m-1,2}$,..., $c_{m-1,\,s_{m-1}}$, the combination of symbol replica candidates for which the accumulated branch metric is assumed to be the smallest is selected, and the calculation of the squared Euclidean distance is repeated S_m times. Thus, this method requires that the squared Euclidean distance be calculated only S_m times, which corresponds to the number of surviving symbol replica candidates at stage m, greatly reducing calculation compared to the conventional QRM-MLD method.

Specifically, while this method has about the same packet error rate and throughput as the Maximum Likelihood Detection (MLD) method (hereinafter referred to as Full MLD method), which does not reduce the amount of calculation, it requires only about 1/1200 of the amount of calculation of the Full MLD method and about 1/4 that of the original QRM-MLD method

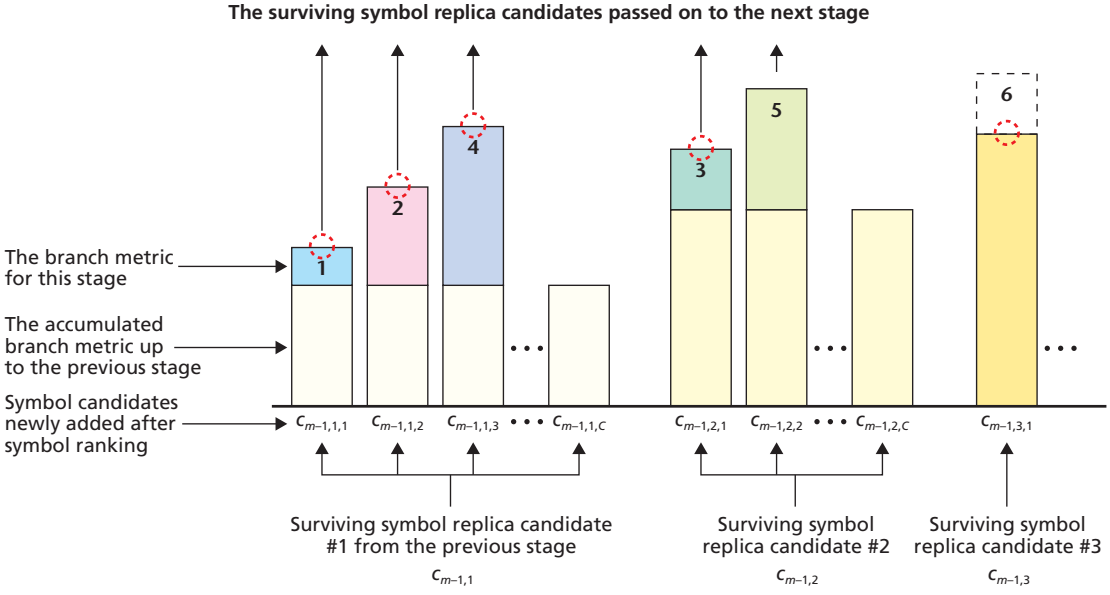

Figure 4 Operative principle of the ASESS

when all of the multiplication, addition and comparison required for signal detection is considered.

2.4 Configuration of the LLR Calculation Unit

In the QRM-MLD method, the number of surviving symbol replica candidates is reduced so as to reduce the amount of calculation. It therefore may happen that there is a "1" or "0 (–1)" bit that has no surviving symbol replica candidate in the final stage of the M-algorithm. To obtain a likelihood for LLR calculation for such bits, a likelihood calculation method based on the accumulated branch metrics of the bits for which there are surviving symbol replica candidates [8] is adopted. The outline of likelihood calculation for bits that have no surviving symbol replica candidates is shown in **Figure 5**. If there are accumulated branch metric calculation results for both bit "1" and "–1," the larger value is selected as the accumulated branch metric and the X multiple of that value averaged within the frame is used as the likelihood of bits for which there is no surviving symbol replica candidate. Furthermore, a method that adopts the difference in Euclidean distance (the square root of the likelihood) is used in the LLR calculation.

3. Laboratory Experiments Results

In the evaluation experiments, four transmitter and receiver antenna branches were used and the QPSK and 16QAM data modulation schemes were adopted. The multipath fading channels between the transmitter and receiver antenna branches were generated by fading simulators. The fading simulator generates a six-path Rayleigh fading signal for which the average received power of each path is decayed 2 dB each, the r.m.s. delay spread, σ, is 0.26 μs, and the maximum Doppler frequency, f_D, is 20 Hz. The Doppler frequency of f_D=20 Hz corresponds to a walking speed of 4.7 km/h. The σ=0.26 μs r.m.s. delay spread is largely based on measurement results obtained in field tests for a cell radius of about 1 km that were conducted in Yokosuka [9].

The transmitted spectrum of the base station equipment and the received spectrum of the input of the mobile station equipment are shown in **Figure 6** (a) and (b) respectively. In the figure, a value of σ= 0.085 μs is used to facilitate understanding of the frequency selective fading conditions. The signal bandwidth is 100 MHz and the reception conditions for the frequency selective (multipath) fading can be seen from the received spectrum. The signal constellations before and after signal detection when 16QAM modulation is used are shown in **Figure 7** (a) and (b) respectively. The signal composed of the signals from the four transmitter antenna branches is received at each of the receiver antenna branches, so the signal positions cannot be

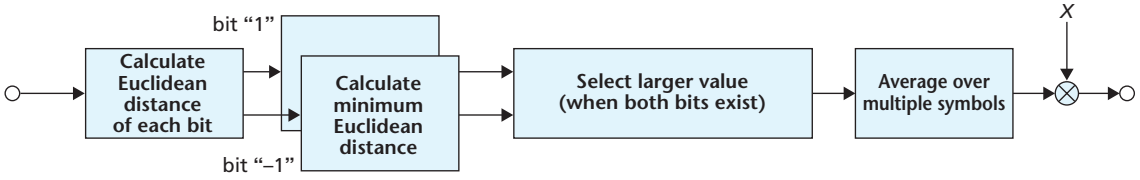

Figure 5 Likelihood calculation for non-existent bits

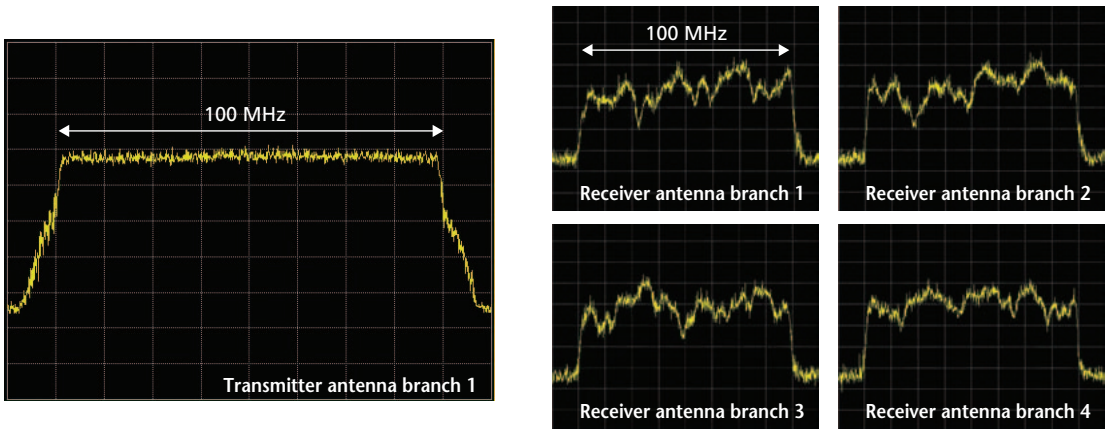

(a) Transmitted spectrum (b) Received spectrum

Figure 6 Transmitted and received spectrums

determined prior to signal detection, but the 16QAM modulation signal constellation is clearly observable after signal detection. Accordingly, we can see that the QRM-MLD signal detection method that applies ASESS is highly accurate.

The packet error rate characteristics for the average received E_b/N_0 per receiver antenna branch with α_{Freq}, the real-valued weighting factor of the MSCA channel estimation filter in the frequency domain, as a parameter are shown in **Figure 8** (a) and (b) for coding rates of R=1/2 and R=8/9, respectively. The real-valued weighting factor in the time domain of α_{Time}=1.0 was selected. For comparison, the results of experiments in which only the pilot symbol of the measured slot is used ($\{\alpha_{Freq}, \alpha_{Time}\}=\{0.0, 0.0\}$, hereinafter referred to as the one-slot channel estimation method) and the results of computer simulations using the same channel model are also shown. For R=1/2 in Fig 8 (a), the average received E_b/N_0 required to satisfy an average packet error rate of 10^{-2} in the experimental results shows a degradation of about 0.5 dB relative to the simulation results, showing that the experimental results are suitably consistent with the simulation results. For R=8/9 in Fig. 8 (b), the experimental results of the average received E_b/N_0 are about 2 dB lower than the simulation results. The large difference in E_b/N_0 relative to the result for

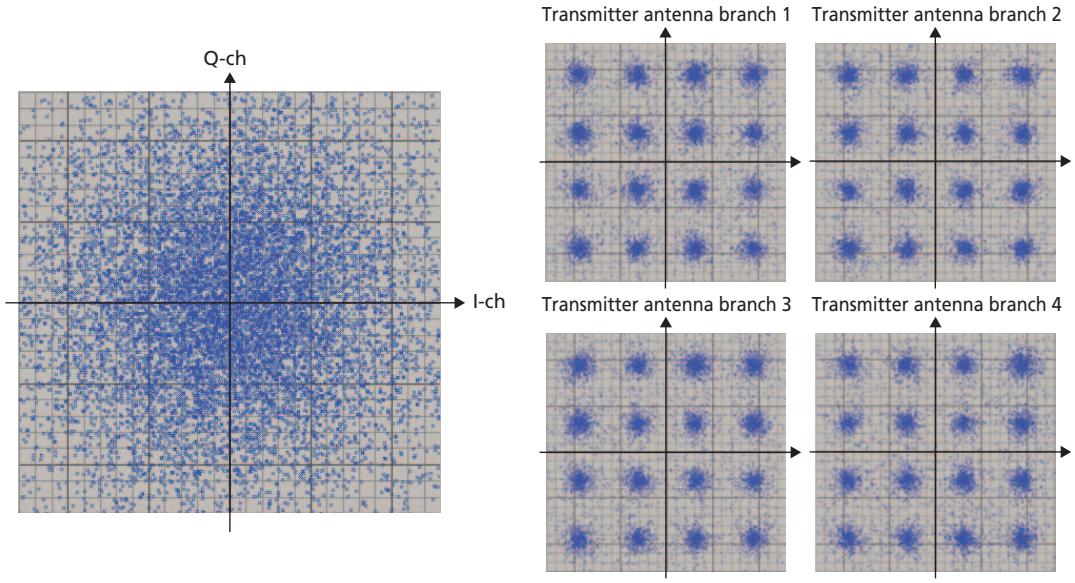

(a) Received constellation (before signal detection)

(b) Received constellation (after signal detection)

Figure 7 Received constellation

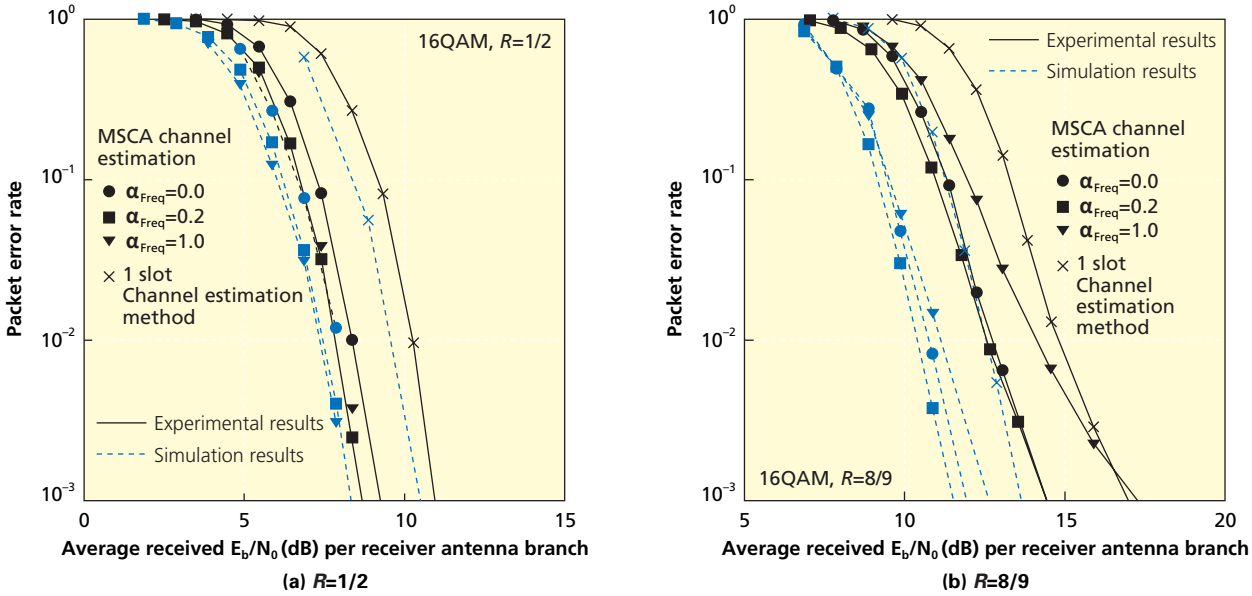

(a) R=1/2

(b) R=8/9

Figure 8 Packet error rate with α_{Freq} as a parameter

R=1/2 is due to the increased effect of the quantization error of the A/D converter because of the higher operating point of the received E_b/N_0. We can see from Fig. 8 (b) that, for a delay spread of σ=0.26 μs, an improvement in the average received E_b/N_0 required to satisfy an average packet error rate of 10^{-2} relative to the one slot channel estimation method can be achieved by applying a $\{\alpha_{Freq}, \alpha_{Time}\}$={0.2, 1.0} MSCA channel estimation filter. This improvement, which is about the same as in the simulation results, has been confirmed by laboratory experiments. The reason for this is that, for low average received E_b/N_0 values, the MSCA channel estimation filter can reduce the effects of background noise by averaging that makes use of the correlations of the previous and next slot and adjacent subcarriers.

The experimental results for the throughput performance for the average received E_b/N_0 per receiver antenna branch when the QRM-MLD method that applies ASESS with R=8/9 is adopted are shown in **Figure 9**. We take the number of surviving symbol replica candidates to be 16 in the first stage (S_1=16) and 28 in the second through fourth stages (S_{2-4}=28). For comparison, the simulation results for the QRM-MLD method with ASESS, the Full MLD method without complexity reduction [10], and the Minimum Mean Squared Error (MMSE) method, all using the same channel model, are also shown. From the simulation results for the QRM-MLD method with ASESS shown in Fig. 9, we see a degradation of less than 0.5 dB relative to the Full MLD method. Furthermore, the QRM-MLD method with ASESS achieves a throughput of 1 Gbit/s at an average received E_b/N_0 of about 12 dB, a reduction in the required average received E_b/N_0 of more than 10 dB compared to the MMSE method. As described above, the largest factor in degradation of the experimental results relative to the simulation results is the quantization noise arising in the A/D converter. It is difficult to consider that this quantization noise has strikingly different effects with respect to computational complexity in the Full MLD method, the QRM-MLD method with ASESS, and the MMSE method. We can therefore assume that the relative differences in performances of the Full MLD method, the QRM-MLD method with ASESS and the MMSE method in the simulation results approximately correspond to differences in their performances assuming implementation of the experimental system.

The average received E_b/N_0 per receiver antenna branch required to satisfy an average packet error rate of 10^{-2} for the likelihood weighting coefficient X for bits that do not exist in the QRM-MLD method with ASESS is shown in **Figure 10**. The LLR computation adopts the Euclidean distance. The figure shows that the most reduction in the required average received E_b/N_0 is obtained for both R=1/2 and R=8/9 when X is in the approximate range of 1.5 to 4.0. The reason for the reduction in the required average received E_b/N_0 when X is greater than one is that better characteristics are obtained when lower likelihood is given for bits that do not exist in the surviving symbol replica candidates in the final stage. The reason that the characteristics deteriorate for X values of four or greater is that it approaches hard-decision turbo decoding. In addition, the near absence of degradation for values of X greater than four in the experimental results is that quantization imposes a limit on the maximum value of the likelihood for non-existent bits.

Finally, the experimental results for the throughput and average received E_s/N_0 (signal energy per symbol-to-noise power spectrum density ratio) performance when {QPSK, R=1/2}, {QPSK, R=2/3}, {QPSK, R=6/7}, {16QAM, R=1/2}, {16QAM, R=2/3}, {16QAM, R=3/4} and {16QAM, R=8/9} are used as the Modulation and channel Coding Scheme (MCS) are shown in **Figure 11**. The computer simulation results for the same conditions are represented by the dotted lines. From Fig. 11 we can see that although the degree of deterioration in the average received E_s/N_0 required to achieve the same throughput relative to the simulation results increases for MCS that provide a higher achievable data rate, even for the 16QAM and R=8/9 MCS, which can achieve a 1.028 Gbit/s data rate, exhibits a degradation of about 2 dB. Furthermore, laboratory experiments have confirmed that using QRM-MLD with ASESS in MIMO multiplexing with four transmitter and receiver antenna branches can attain throughputs of 500 Mbit/s, 800 Mbit/s and 1 Gbit/s for average received E_s/N_0 values of 9.5 dB, 13.5 dB, 17.5 dB when {16QAM, R=1/2}, {16QAM, R=3/4} and {16QAM, R=8/9} MCS are used.

4. Conclusion

We described the configuration of an experimental 1-Gbit/s packet signal transmission system that applies MIMO multiplexing in a VSF-Spread OFDM radio access that has a 100 MHz downlink frequency bandwidth. We have also reported the results of laboratory experiments in which a multipath fading simulator was used. The experimental results show that 1-Gbit/s packet signal transmission (frequency efficiency of 10 bit/s/Hz) can be achieved at an average received E_b/N_0 of about 12 dB by

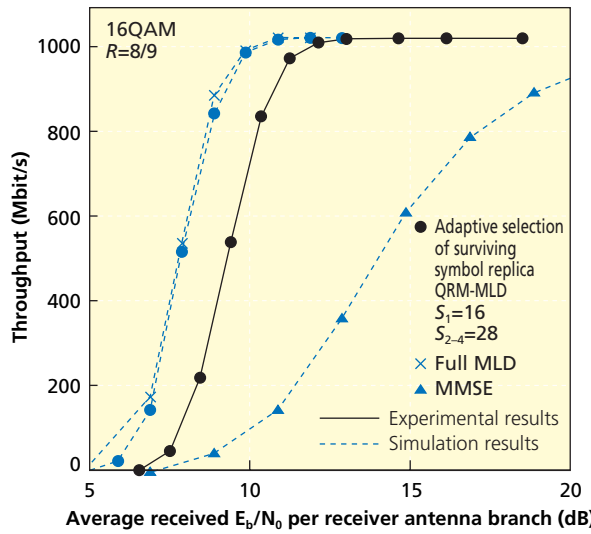

Figure 9 Throughput performance of QRM-MLD with adaptive selection of surviving symbol replica

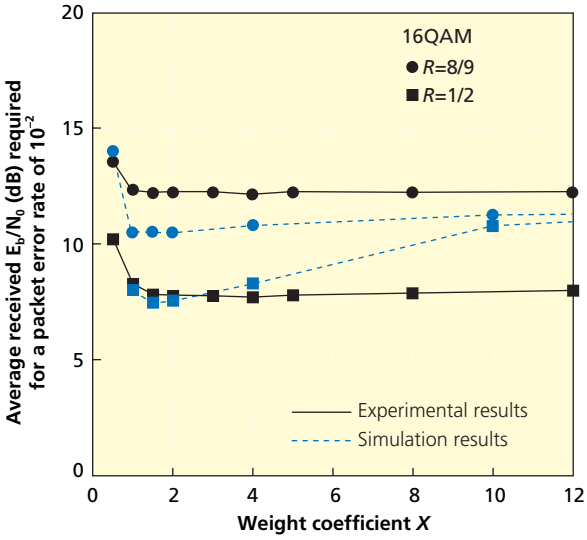

Figure 10 Dependency of required average received E_b/N_0 on weight coefficient *X*

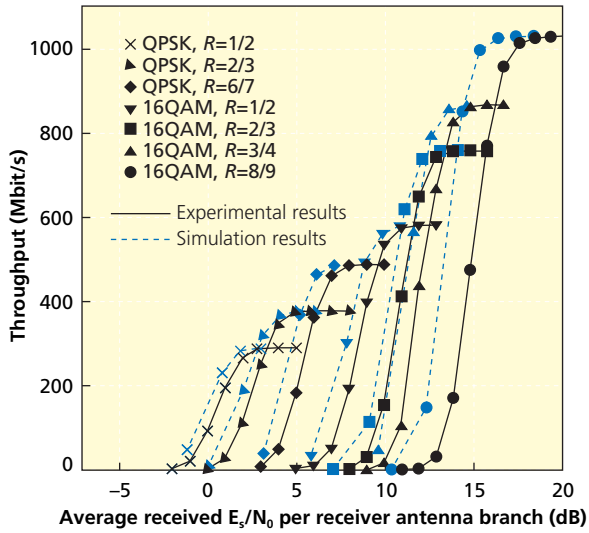

Figure 11 Throughput performance for each MCS

using MIMO multiplexing with four transmitter and receiver antenna branches, a QRM-MLD signal detection method that adopts ASESS, 16QAM data modulation, soft-decision Turbo decoding with a coding rate of 8/9.

References

[1] G. J. Foschini, Jr.: "Layered space-time architecture for wireless communication in a fading environment when using multi-element antennas," Bell Labs Tech. J., pp. 41–59, Autumn 1996.

[2] R. D. Murch and K. B. Letaief: "Antenna Systems for Broadband Wireless Access," IEEE Commun. Mag., Vol. 40, No. 4, pp. 76–83, Apr. 2002.

[3] H. Atarashi, S. Abeta and M. Sawahashi: "Variable spreading factor orthogonal frequency and code division multiplexing (VSF-OFCDM) for broadband packet wireless access," IEICE Trans. Commun., Vol. E86-B, No. 1, pp. 291–299, Jan. 2003.

[4] T. A. Thomas, K. L. Baum and F. W. Vook: "Modulation and coding rate selection to improve successive cancellation reception in OFDM and spread OFDM MIMO systems," Proc. IEEE ICC 2003, pp. 2842–2846, May 2003.

[5] H. Kawai, K. Higuchi, N. Maeda and M. Sawahashi: "Performance of QRM-MLD employing two-dimensional multi-slot and carrier-averaging channel estimation using orthogonal pilot channel for OFCDM MIMO multiplexing in multipath fading channel," Proc. Wireless2004, pp. 208–214, Jul. 2004.

[6] K. Higuchi, H. Kawai, N. Maeda and M. Sawahashi: "Adaptive Selection of Surviving Symbol Replica Candidates Based on Maximum Reliability in QRM-MLD for OFCDM MIMO Multiplexing," Proc. IEEE Globecom 2004, pp. 2480–2486, Nov. 2004.

[7] K. J. Kim, J. Yue, R. A. Iltis and J. D. Gibson: "A QRD-M/Kalman filter-based detection and channel estimation algorithm for MIMO-OFDM systems," IEEE Trans. Wireless Commun., Vol. 4, No. 2, pp. 710–721, Mar. 2005.

[8] K. Higuchi, H. Kawai, N. Maeda, M. Sawahashi, T. Itoh, Y. Kakura, A. Ushirokawa and H. Seki: "Likelihood function for QRM-MLD suitable for soft-decision turbo decoding and its performance for OFCDM MIMO multiplexing in multipath fading channel," Proc. IEEE PIMRC2004, pp. 1142–1148, Sep. 2004.

[9] H. Atarashi, Y. Kishiyama, N. Maeda, N. Miki, K. Higuchi and M. Sawahashi: "Field experiments on throughput performance above 100 Mbps in forward link for VSF-OFCDM broadband wireless access," Proc. ISSSE2004, Aug. 2004.

[10] A. van Zelst, R. van Nee and G. A. Awater: "Space division multiplexing (SDM) for OFDM systems," Proc. IEEE VTC2000-Spring, pp. 1070–1074, May 2000.

ABBREVIATIONS

AGC: Automatic Gain Control
BPF: Band Pass Filter
FFT: Fast Fourier Transform
GI: Guard Interval
IF: Intermediate Frequency
IFFT: Inverse Fast Fourier Transform
LLR: Log Likelihood Ratio
LNA: Low Noise Amplifier
MAP: Maximum A Posteriori
MCS: Modulation and channel Coding Scheme
MIMO: Multiple Input Multiple Output
MLD: Maximum Likelihood Detection
MMSE: Minimum Mean Squared Error
MSCA: Multi-Slot and sub-Carrier Averaging
OFDM: Orthogonal Frequency Division Multiplexing
QAM: Quadrature Amplitude Modulation
QPSK: Quadrature Phase Shift Keying
QRM-MLD: complexity-reduced Maximum Likelihood Detection with QR decomposition and M-algorithm
RF: Radio Frequency
S/P: Serial-to-Parallel conversion
VSF: Variable Spreading Factor